10.1002/cphc.201900565

WILEY-VCH

COMMUNICATION

Cu^{2+} effects on beta-amyloid oligomerisation monitored by fluorescence of intrinsic tyrosine

Abeer Alghamdi[a], Thorben Wellbrock[a], David J.S. Birch[a], Vladislav Vyshemirsky[b], and Olaf J. Rolinski*[a]

Abstract: A non-invasive intrinsic fluorescence sensing of the early stages of Alzheimer's beta amyloid peptide aggregation in the presence of copper ions is reported. By using time-resolved fluorescence techniques the formation of beta amyloid-copper complexes and the accelerated peptide aggregation are demonstrated. The shifts in the emission spectral peaks indicate that the peptides exhibit different aggregation pathways than in the absence of copper.

Certain proteins are prone to aggregation which may lead to the disease of amyloidosis, e.g. β-amyloid and Alzheimer's disease (AD), α-synuclein and Parkinson's disease, or islet amyloid polypeptide and type II diabetes. Proteins specific to each disease form stable and insoluble amyloid plagues, which deposit in the body, but it is the smaller precursor oligomers which possess potential redox activity and that interfere with cell membrane, disturbing its functions and leading to cell death. Great attention has been given in recent years to β-amyloid ($A\beta_{1-40}$ and $A\beta_{1-42}$ peptides), because AD is the most common of the neurodegenerative disorders, afflicting 5% of men and 6% of woman over 60 years of age, and currently it has no cure. Given the aging nature of our society, it is clear, that AD constitutes one of the major health issues of our time.
Extracellular amyloid plaques composed mainly of $A\beta_{1-40}$ and $A\beta_{1-42}$ fibrils are morphological hallmarks of Alzheimer's disease. According to the amyloid cascade hypothesis[1–3], the increase in Aβ production and/or accumulation lead first to the formation of Aβ oligomers, then to protofibrils and ultimately to insoluble amyloid fibrils. According to this hypothesis, the neurotoxicity and synaptotoxicity may be mediated by the soluble oligomers of Aβ. However, the mechanism of Aβ toxicity is poorly defined and remains a controversial topic in the field.

[a] A. Alghamdi, T.Wellbrock, Prof. D.J.S.Birch, Dr O.J. Rolinski
Department of Physics
University of Strathclyde, Glasgow G4 0NG (UK)
E-mail: o.j.rolinski@strath.ac.uk
[b] Dr V.Vyshemirsky
School of Mathematics and Statistics
University of Glasgow, Glasgow G12 8QQ (UK)

Supporting information for this article is given via a link at the end of the document.

Metal ions such as Cu^{2+} and Zn^{2+} are found in abnormally high concentrations within senile plaques of Alzheimer's. In vitro studies[4,5] show that such ions can bind to Aβ directly and modulate the aggregation process. Given the redox activity of Cu it is strongly believed that its complex with Aβ (Cu-Aβ) might be involved in the formation of reactive oxygen species[5] that contribute to the oxidative stress observed in Alzheimer's disease. Thus, it appears that the interaction of Cu with Aβ is linked to Alzheimer's disease.
Cu-Aβ complexes have been investigated widely for the past decade by means of various techniques including IR spectroscopy[6], x-ray absorption spectroscopy XAS[6,7], circular dichroism CD[7,8], Nuclear Magnetic Resonance NMR[7], Raman spectroscopy[9] and Electron Paramagnetic Resonance EPR[7,8]. Currently, the most accepted coordination model of Cu^{2+} ions to the Aβ peptide at pH 7.4 suggests that the Cu-Aβ complex can exist in two main forms[10-12] as shown in Fig.1. The two components are usually noted I and II. In component I, Cu^{2+} preferably binds to the -NH2 terminal amine, the adjacent CO from the Asp1-Ala2

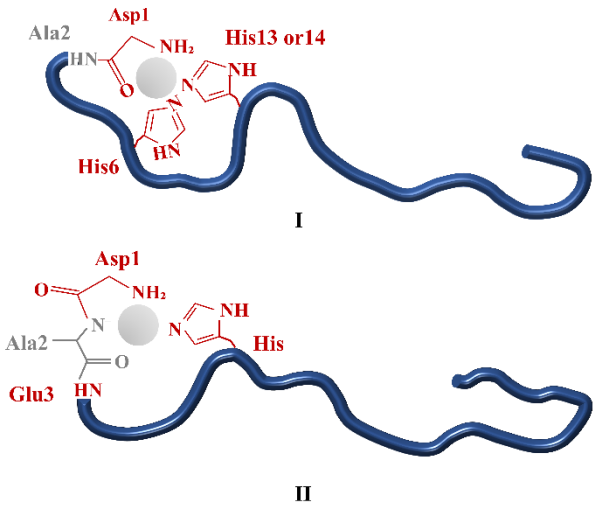

peptide

Fig. 1 Scheme showing the coordination sites of Cu^{2+}-Aβ for component I and II at pH 7.4.

bond, the N atom from the imidazole ring of His6 and imidazole ring of His13 or His14, or two N atoms from

His13 and His14. The apical position of the square-pyramidal copper complex is likely to be occupied by an oxygen atom from either a carboxylate group or a water molecule. Component II can be generated by the deprotonation of the Asp1-Ala2 amide bond, which leads to Cu^{2+} binding equatorially to the deprotonated amide function from the Asp1-Ala2 peptide bond, the N-terminal amine, the adjacent CO from Ala2-Glu3 peptide bond and one N atom from the imidazole ring of either His6, His13 or His14.
The extensively discussed aspect of the role of copper in Alzheimer's is its impact on the aggregation of Aβ in the presence of Aβ-Cu^{2+} complexes[10]. The formed aggregates are either amorphous or fibrillar and both depend on experimental parameters such as the concentration of Cu^{2+} and the pH level. It has been suggested that Cu^{2+} ions accelerate the formation of fibrils at the 1:1 ratio, possibly due to metal-mediated dimerization and a stabilization of oligomers[10]. Conversely, excess amounts of Cu^{2+} produces more amorphous aggregates and less fibrils.

Here we report the non-invasive sensing of the early stages of Aβ aggregation in the presence of Cu^{2+} ions by monitoring the fluorescence responses of its intrinsic amino acid Tyrosine. Fluorescence time-resolved spectroscopy of intrinsic fluorophores in biological systems is unique in offering sub-nm spatial and sub-ns time resolution, allowing determination of biomolecular structures and their functions. We have recently demonstrated[13,14], that exploiting an Å spatial and ns temporal scales of intrinsic fluorophores offers a new approach to understanding the processes leading to misfolding and aggregation of $A\beta_{1-40}$. Peptide $A\beta_{1-40}$ is an ideal model system for intrinsic fluorescence-based studies, as it contains no tryptophans and only one tyrosine (Tyr_{10}), which can be excited individually and provide clear information on the changes in its local environment, which makes it an efficient and non-invasive (no need for dye labelling) sensor of aggregation. We have found[15], that Tyr fluorescence decay in $A\beta_{1-40}$ is well represented by a multi-exponential function during the whole process of aggregation, which may be consistent with the protein model of rotamers. The evolution of the parameters of multi-exponential decays can serve as an indication of the current stage of oligomerisation. The rate and performance of the process have been found to depend on the initial $A\beta_{1-40}$ concentration, buffer, presence of additives and label dyes. We have also shown[16], that our approach for detecting $A\beta_{1-40}$ aggregation has the highest sensitivity at the initial stages of aggregation (monomer-monomer, monomer-dimer, etc), contrary to the traditional technique based on thioflavin T (ThT), which fluorescence intensity increases when aggregation reaches the state of β-sheet formation. Similarly, the light scattering as the method for detecting amyloid aggregates is only efficient at the later stages, when the aggregates achieve larger sizes.

More recently, we have established[17] that time resolved emission spectra (TRES) of Tyr in $A\beta_{1-40}$ can sufficiently demonstrate structural changes on the nanosecond time scale after excitation. Beta-amyloid's monomers can be distinguished from oligomers by means of the position of their emission spectra. Further spectral shift caused by dielectric relaxation can be useful for determining the size of the oligomers since their spectral shift gradually decreases as the aggregates grow larger.
In this paper we use for the first time our non-invasive technique to research $A\beta_{1-40}$ interactions with copper ions and consequent aggregation of the copper – bound amyloids, making the next step towards better understanding of neurotoxicity of amyloid oligomers. Our approach explores the relationship between the changes in intrinsic fluorescence of Tyr_{10} in $A\beta_{1-40}$ and the progress of $A\beta_{1-40}$ aggregation[13,14,16,18] . Thanks to the non-invasiveness of the Tyr_{10}-based approach we achieve a perhaps unique opportunity to detect the earliest stages of $A\beta_{1-40}$ –Cu^{2+} interactions, well before the other techniques detect any changes.
To allow the interpretation of the Tyr in $A\beta_{1-40}$ decay data in the context of copper impact on aggregation, we extended the lifetime measurements to the number of samples with Tyr-containing amyloid fragments and copper, and gradually increased the level of their complexity (sequentially: Tyr, N-Acetyltyrosinamide (NAYA), $A\beta_{1-16}$, $A\beta_{1-40}$).
Free Tyr in buffered water shows simple exponential kinetics, which produces an excellent starting point for the lifetime studies. However, in the heterogeneous fluorescent systems like aggregating $A\beta_{1-40}$ peptides, where several processes affecting excited-state kinetics (like variable tyrosine local environments and/or dielectric relaxation) may be present, measuring the fluorescence decay at a single and arbitrary selected detection wavelength may not be sufficient to describe such a complex kinetics. For these cases the complementary technique such as time resolved emission spectra (TRES) may provide additional information. Indeed, the shape of the $A\beta_{1-40}$ spectrum at different moments of time after excitation and the way it evolves on the ns time scale may help to resolve the number of fluorescent sites involved and reveal the actual kinetics. Therefore, in this research we used both, fluorescence intensity decays and TRES, to maximise information on $A\beta_{1-40}$ behavior.

Copper in the solutions of Aβ fragments can potentially cause two types of effects on fluorescence kinetics: direct, i.e. quenching of Tyr fluorescence and indirect, by having the influence on aggregation process. The potential direct effects were investigated first. Adding mM concentrations of Cu^{2+} reduces the value of Tyr's fluorescence lifetime τ as shown in Fig. 2a. The ratio τ_o/τ , where τ_o is the lifetime of Tyr without Cu^{2+}, follows the Stern-Volmer relationship, i.e. is

10.1002/cphc.201900565

proportional to the concentration of Cu^{2+} (Fig. 2b), indicating collisional quenching. However, at the concentrations of Cu^{2+} ions in the μM range i.e. similar to the concentration of Aβ (50 μM) used in our experiments, τ remains constant (Fig. 2c), which excludes collisional quenching of Trp by Cu^{2+} in μM range. The next step was to investigate the influence of Cu^{2+} on NAYA, which is considerably an appropriate model compound of a nonterminal tyrosine within a protein. Fluorescence decay of Tyr in NAYA is intrinsically more complex and well described by a two-exponential model. Adding Cu^{2+} to NAYA did not affect the lifetime components and their contributions as we increased the concentration of Cu^{2+} up to 100 μM (Fig. 2d and e). Therefore, it is reasonable to accept that the fluorescence kinetics of NAYA is also not affected by Cu^{2+}. The $A\beta_{1\text{-}16}$ fragment was then investigated upon adding μM concentrations of Cu^{2+}. Due to increasing complexity of the local environment of Tyr in this peptide, obtaining a good fit for fluorescence decay for the no-Cu^{2+} sample required using a 3-exponential model. The fitted decay times and their associated contributions change with Cu^{2+} concentration as shown in Fig. 2f and g. The effect observed is likely to be a result of the Cu^{2+}-Aβ complex formation, as His6 and His13 (or His14) are expected to form copper ion binding site in $A\beta_{1\text{-}16}$ peptide. This explains why Tyr's fluorescence signal in $A\beta_{1\text{-}16}$ is considerably sensitive to the change in Cu^{2+} concentration. Overall, the effect of binding to Cu^{2+} is weak.

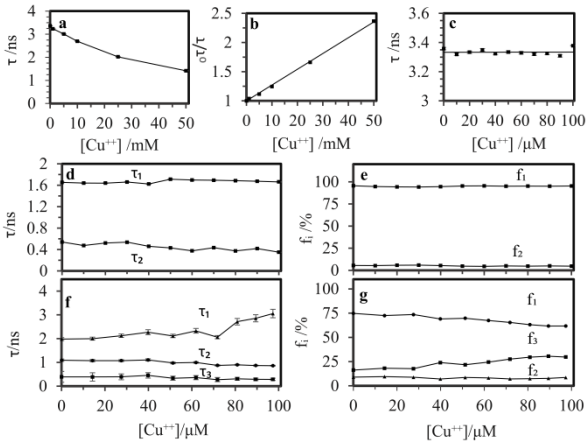

Fig. 2 Plots showing the correlation between Tyr's Fluorescence lifetime τ and the concentration of Cu^{2+} in mM (a) and μM (c) scales; The Stern–Volmer plot of fluorescence quenching of Tyr by Cu^{2+} ions (b); Plot showing the effect of Cu^{2+} on parameters obtained from fitting NAYA's fluorescence decay to a two-exponential model: decay times τ_1 and τ_2 (d), and the percentage contributions f_1 and f_2 (e); Parameters obtained from fitting Tyr's fluorescence decay in a 50 μM $A\beta_{1-16}$ solution to a three-exponential decay model plotted against Cu^{2+} concentration: Tyr fluorescence decay times τ_1, τ_2 and τ_3 (f), percentage contributions f_1,f_2 and f_3 (g). Error bars represent the standard deviation.

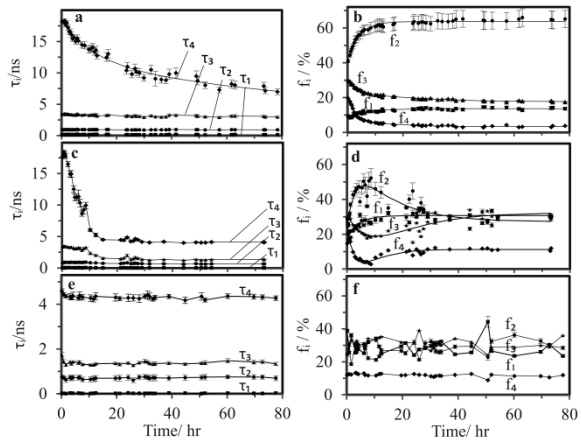

Fig. 3 Parameters obtained from fitting Tyr fluorescence decay in a 50 μM $A\beta_{1-40}$ solution to a four-exponential decay model as aggregation proceeds: Tyr fluorescence decay times τ_1, τ_2, τ_3 and τ_4 in free $A\beta_{1-40}$ (a), in the presence of 15 μM (c) and 35 μM (e) of Cu^{2+}, percentage contributions of the decay components f_1, f_2, f_3 and f_4 in free $A\beta_{1-40}$ (b), in the presence of 15 μM (d) and 35 μM (f) of Cu^{2+}. Error bars represent the standard deviation.

The copper ions effects on the full Alzheimer's peptide, $A\beta_{1\text{-}40}$, were studied by monitoring fluorescence responses of three samples: one without copper and the other two containing 15 μM and 35 μM of Cu^{2+}. The samples were prepared according to the procedure minimizing the number of oligomers in the initial sample[19] (see Supporting Information for details). Measurements were taken several times over the period of 80 hours to track the evolution in the Tyr signal. The $A\beta_{1\text{-}40}$'s fluorescence intensity decays were best fitted to the 4-exponential model functions. Figs. 3a and b show the changes in the lifetime components and percentage contributions as the $A\beta_{1\text{-}40}$ sample aggregation progresses in the absence of Cu^{2+} ions. Three of the lifetime components ($\tau_1 \approx 0.1$ ns, $\tau_2 \approx 1$ ns and $\tau_3 \approx 3.4$ ns) remain constant during the aggregation process whereas the forth τ_4 exhibits a significant decrease from 18 ns to 8 ns within 80 hours. The contributions of the two short lifetime components f_1 and f_2 show an increase in the first 15 hours and then remain constant as the aggregation progresses (Fig. 3b). Simultaneously, the contributions of the two components with larger lifetimes, f_3 and f_4, exhibit an initial decrease and then remain the same as the sample ages. Changes observed in the fluorescence decay parameters suggest conformational changes in $A\beta_{1\text{-}40}$ during its aggregation and can be used to indicate the

stage of peptide aggregation, as we have done previously[13].

Fig. 3c shows the developments in lifetime components of $A\beta_{1-40}$ in the presence of 15 μM of Cu^{2+}. Note, that the initial values of $\tau_1 \div \tau_4$ are identical to those obtained in the absence of Cu^{2+}. This demonstrates, that at the beginning of aggregation the presence of copper ions does not affect the excited-state fluorescence kinetics of Tyr in $A\beta_{1-40}$. Later changes in the fluorescence decays of 15 μM Cu^{2+} sample are different than observed in a no-Cu^{2+} sample. The decay times $\tau_1 \div \tau_3$ remain constant only for the first 10 hours and then they decay to $\tau_1 \approx 0.01$ ns, $\tau_2 \approx 0.6$ ns and $\tau_3 \approx 1.4$ ns within the next 5 hours and remain constant afterwards (see also Fig S4). The lifetime of the fourth component decays at a faster rate than that observed in free $A\beta_{1-40}$ from 18 ns to 4 ns within 10 hours. Simultaneously, the contributions of the decay components $f_1 \div f_4$ show similar behavior to that observed in free $A\beta_{1-40}$ for the first 10 hours only and then this trend breaks down (Fig. 3d). The lifetimes and contribution parameters taken together suggest that during the first 10 hours the aggregation occurs in a similar way as in a no-Cu^{2+} sample. After this time the complexation accelerates and the structure of the final product is different than the structure created in the absence of Cu^{2+}. Decreases in all four lifetime parameters of the Cu^{2+}-containing sample seems to explain the quenching of fluorescence observed in the previous steady-state studies of similar systems[20].

In the presence of 35 μM concentration of Cu^{2+} (Fig. 3e and f), the decay times along with the associated relative contributions are fairly constant during the time of experiment and their values are almost identical to those obtained for the 15 μM Cu^{2+} sample after around 15 hours. This suggests that the aggregation occurring in the 35 μM Cu^{2+} sample is similar to the process in the 15 μM Cu^{2+} sample but is significantly accelerated.

To summarize this section, the analysis of Tyr fluorescence decays shows that copper ions not only accelerate the aggregation of $A\beta_{1-40}$ peptides but also alter the final products (oligomers). Indeed, decreasing values of all lifetime parameters τ_i and changes in the f_i contributions observed after the 10th hour of aggregation in the 15 μM Cu^{2+} sample, may be the result of radical alterations in the immediate environment of the Tyr residues.

We also note, that because adding copper ions affects all τ_i and f_i parameters in a similar manner, a 4-exponential function used in data analysis is unlikely to reflect a 4-rotamer kinetics of Tyr in $A\beta_{1-40}$ but is only a good analytical representation of the decays. Moreover, it is not clear if fluorescence intensity decays collected at one arbitrarily selected detection wavelength efficiently reflect the kinetics of this undoubtedly complicated molecular system.

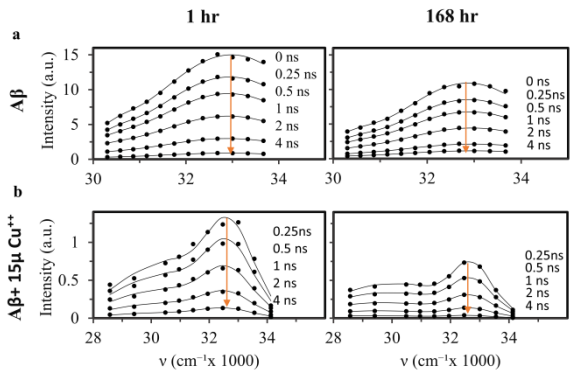

Fig. 4 Time-resolved emission spectra (TRES) obtained for 50 μM $A\beta_{1-40}$ (a) and 50 μM $A\beta_{1-40}$ with 15 μM Cu^{2+} (b) at two stages of aggregation (1 hr and 168 hr). The solid lines represent the two-Toptygin type functions fits.

Therefore, to reveal more information on the underlying kinetics, TRES measurements were performed for $A\beta_{1-40}$ at several stages of aggregation, namely 1, 5, 24, 48, 72, 96 and 168 hrs after sample preparation (the number indicates the age of the sample when the measurement at the first wavelength has been started).

Fig. 4 shows the examples of TRES of the 1 hour and 168 hours old samples without (Fig. 4a) and with 15 μM (Fig. 4b) of copper ions. According to Toptygin and Brand[21] the fluorescence spectrum of a single fluorescent residue can be expressed as $\sim\nu^3 g(\nu)$, where $g(\nu)$ is the Gaussian distribution function. Therefore, for the purpose of detailed analysis of the $A\beta_{1-40}$ TRES we modelled the recovered spectra $I_t(\nu)$ at the time t as the sum of N normalized functions of the type $\sim\nu^3 g(\nu)$, namely:

$$I_t(\nu) = \sum_{i=1}^{N} \frac{C_i(t)\nu^3 \exp\left[-\left(\nu-\nu_i(t)\right)^2/\left(2\sigma_i^2(t)\right)\right]}{(2\pi)^{1/2}\nu_i(t)\sigma_i(t)\left(\nu_i^2(t)+3\sigma_i^2(t)\right)} \quad (1)$$

Here t is the time after excitation in ns, ν is wavenumber in cm^{-1}, $\sigma_i(t)$ is the standard deviation of each component, $\nu_i(t)$ is its peak position and $C_i(t)$ - the fluorescence contribution of the i-th component at the time t, i.e. its fluorescence intensity decay.

In our previous work[17] on aggregation of free $A\beta_{1-40}$ we have identified two peaks in the spectra and explained them by the presence of non-aggregating monomers and aggregating oligomers, both involved in

10.1002/cphc.201900565

dielectric relaxation at different rates. The analysis of the experimental TRES for the sample with Cu^{2+} also demonstrated the presence of two components (N=2).

Here we compare the fluorescence kinetics of the both samples, one without Cu^{2+} and one with 15 μM of Cu^{2+} ions by means of the parameters recovered from fitting the model TRES (eqn 1 for N=2) to the experimental data (Fig. 5). In the absence of Cu^{2+} (Fig. 5a) the position of the first peak $\nu_1(t)$ is located at about 33000 cm^{-1} and does not show significant changes over time, which indicates fast dielectric relaxation that is practically completed before fluorescence occurs. Therefore we attribute this component to the monomers. The second peak starts from an initial value $\nu_2(0)\approx$ 30500 cm^{-1} and, for the 1 hr old sample, shows an exponential shift to a lower energy value $\nu_2(\infty)\approx$ 29000 cm^{-1} with the dielectric relaxation time τ_R = 6.7 ns . The relaxation time increases as the sample ages indicating gradual growth in the aggregates size. We associate the second peak with oligomers because it justifies why it initially appears at a lower energy value (30500 cm^{-1}) due to aggregation and its further red shift due to dielectric relaxation.

Addition of 15 μM Cu^{2+} to the sample (Fig. 5b) shifts only slightly the position of the first peak $\nu_1(t)$ from 33000 cm^{-1} to 32800 cm^{-1}. No further shift is observed after excitation and remains unchanged as the sample ages. This is consistent again with fast relaxation of the non-aggregated monomers. The second peak, on the other hand, is sensitive to the stage of aggregation, i.e. the initial positions of the

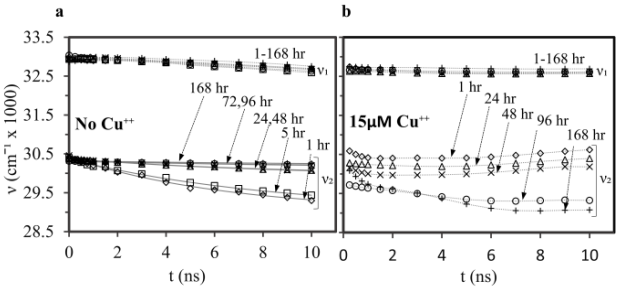

Fig. 5 Evolution of the peak positions ν_1 (t) and ν_2 (t) for free $A\beta_{1\text{-}40}$ (a) and Aβ1−40 with 15 μM Cu^{2+} (b) at different stages of aggregation (◊ 1hr, □ 5hr, Δ 24hr, × 48hr, ∗ 72hr, ○ 96 hr and + 168 hr).

peak gradually shift from around 30600 cm^{-1} to 30000 cm^{-1} within 169 hrs. The positions of the peak $\nu_2(t)$ of the sample at different ages exhibit an initial decrease followed by an increase after about 6 ns. Such behavior suggests that it represents at least two types of aggregates with each having different peaks of emission spectra and different decay rates. In older samples (>96 hours) $\nu_2(t)$ has no increasing stage, which indicates again the fluorescence of one rather than two fluorescent species. This may be explained by larger aggregates having very low fluorescence emission due to reabsorption or by precipitation of the larger fibrils.

The analysis of the $C_1(t)$ and $C_2(t)$ functions obtained for both samples (Fig. 6) provides additional clues. In the free $A\beta_{1\text{-}40}$ sample the $C_1(t)$ (monomers, Fig. 6a) decays in the similar way

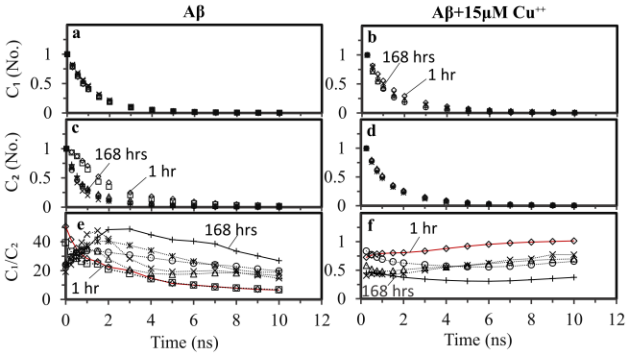

Fig. 6 Fluorescence intensity decay of the two components C_1(t) and C_2(t) for free $A\beta_{1\text{-}40}$ (a,c) and $A\beta_{1\text{-}40}$ with 15 μM of Cu^{2+} (b,d); The ratio of the monomer to oligomer contribution C_1(t)/C_2(t) plotted against time for free $A\beta_{1\text{–}40}$ (e) and $A\beta_{1\text{–}40}$ in the presence of 15 μM of Cu^{2+} (f) at different stages of aggregation (◊ 1hr, □ 5hr, Δ 24hr, × 48hr, ∗ 72hr, ○ 96 hr and + 168 hr);

irrespectively of the age of the sample, while the character of the $C_2(t)$ (oligomers, Fig. 6c) alters when sample ages. The initial ratio $C_1(0)/C_2(0)$ (Fig. 6e) demonstrates the domination of the monomer's emission, which decreases as the sample ages due to oligomer formation. We note that the $C_1(t)/C_2(t)$ plots are highly sensitive to the stage of aggregation, and thus can be used as indicators of $A\beta_{1\text{-}40}$ aggregation stage.
The decays $C_1(t)$ and $C_2(t)$ in the copper containing sample (Fig. 6b, d, and f) show that the character of $A\beta_{1\text{-}40}$ aggregation is dominated by the presence of copper ions from the very beginning. The characters of the decays $C_1(t)$ and $C_2(t)$ are similar and do not change substantially while the sample ages (Fig. 6b and d). The ratio $C_1(t)/C_2(t)$ is substantially smaller and quite stable as compared to the no-Cu^{2+} sample and decreases with sample aging. Moreover, the contribution of the second peak is significantly higher than that observed in free $A\beta_{1\text{-}40}$ (Fig. 6e, f), which suggests that the formation of Aβ aggregates is intensively triggered by Cu^{2+}. The contribution of the second peak slightly increases as the sample ages. This might be a result of large aggregate precipitation or because of their low quantum yields.

To conclude, the time-resolved studies of free Tyr and Tyr in Aβ fragments show that Cu^{2+} at μM concentrations does not quench Tyr fluorescence. The

formation of Cu^{2+}-Aβ_{1-40} complexes, however, substantially accelerates the process of peptide aggregation. TRES measurements show that Aβ aggregates in the presence of Cu^{2+}, exhibit considerable shifts in their emission peak during peptide aggregation. Such behavior suggests that Aβ_{1-40} peptides exhibit different aggregation pathways and form different types of aggregates when Cu^{2+} is present.

We believe that the observed substantial differences in the Aβ_{1-40} and Aβ_{1-40}-Cu^{2+} time-resolved fluorescence responses offer the possibility for identifying different types of amyloid aggregates induced by the presence of specific factors, e.g. sugars (glycation), environmental conditions, anti-aggregation compounds, etc. The TRES parameters recovered in our approach can be used to propose a possibly broad selection of the potential models of the kinetics. Determining the specific type of aggregates would be then based on the best-fitting kinetic model and values of its parameters. Due to the expected complexity of these models, their numerical solutions would have to be calculated and fitted to the experimental decays. Our preliminary attempts to fit the numerical model solutions to the experimental decay data demonstrate the full feasibility of such an approach. This strategy can be beneficial for all complex biological systems, where the dogmatic use of multi-exponential models of the decays can be inefficient and not insightful.

Keywords: beta-amyloid aggregation • copper ions • Alzheimer's disease • TRES • protein intrinsic fluorescence

[1] E. Karran, M. Mercken, B. De Strooper, *Nat Rev Drug Discov.* **2011**, 10, 698.

[2] J. Hardy, *J. Neurochem.* **2009**, 110, 1129.

3. P. Faller, *ChemBioChem.* **2009**, 10, 2837.

4. Al Bush, *Trends in neurosciences* **2003**, 26, 207.

5. P.A. Adlard , Bush AI, *J Alzheimer's Dis*. **2006**, 10, 145.

6. V. Minicozzi, F. Stellato, M. Comai, M. Dalla Serra, C. Potrich, W Meyer-Klaucke, et al *J Biol Chem.* **2008**, 283, 10784.

7. C. Hureau, *Coord. Chem. Rev.* **2012**, 256, 2164.

8. P. Faller, C. Hureau, *Dalton Trans.* **2009**, 7, 1080.

9. J. Dong, C. S. Atwood, V. E. Anderson, S. L. Siedlak, M. A. Smith, G. Perry, et al *Biochemistry* **2003**, 42, 2768.

10. V. Borghesani , B. Alies, C. Hureau, **2018** *Eur. Jour. Inorg. Chem.* **2018**, 7,15.

11. T. Branch, P. Girvan, M. Barahona, L. Ying, *Angew. Chem. Int. Ed.* **2015**, 54, 1227.

12. J. T. Pedersen, K. Teilum, N. H. H. Heegaard, J. Østergard, H. W. Adolph, L. Hemmingsen, *Angew. Chem. Int. Ed.* **2011**, 50, 2532.

13. O. J. Rolinski, M. Amaro, D J. S. Birch *Biosens. Bioelectron.* **2010**, 25, 2249.

14. M. Amaro, T. Wellbrock, D.J.S. Birch, O.J. Rolinski *Appl Phys Lett* **2014**, 104, 063704.

15. O.J. Rolinski, T. Wellbrock, D.J.S. Birch, V. Vyshemirsky *J Phys Chem Lett* **2015**, 6, 3116–20.

16. M. Amaro, D.J.S. Birch, O. J. Rolinski *Phys Chem Chem Phys* **2011** 13, 6434.

17. A. Alghamdi, V. Vyshemirsky, D.J.S. Birch DJS, O.J. Rolinski *Methods Appl Fluoresc* **2018** 6, 024002.

18. M. Amaro, K. Kubiak-Ossowska, D.J.S. Birch, O. J. Rolinski *Methods Appl Fluoresc* **2013**, 1, 015006.

19. W. B. Stine, K. N. Dahlgren, G. A. Krafft, & M. J. LaDu *J Biol Chem* **2003**, *278*, 11612-22.

20. B.Alies, E.Renaglia, M.Rozga, W.Bal, P.Fallen, C.Hureau, *Anal Chem* 2013, 85 1501-1508.

21. D.Toptygin, L.Brandt, *Chem.Phys.Lett* **2000**, 322, 496.

10.1002/cphc.201900565

Entry for the Table of Contents (Please choose one layout)

Layout 1:

COMMUNICATION

Text for Table of Contents

*Author(s), Corresponding Author(s)**

Page No. – Page No.

Title

10.1002/cphc.201900565